Energy Balance in a Laser-Induced Forward Transfer Process Studied by Shadowgraphy†

Romain Fardel,‡,§ Matthias Nagel,‡ Frank Nüesch,‡ Thomas Lippert,*,§ and Alexander Wokaun§

Empa, Laboratory for Functional Polymers, Swiss Federal Laboratories for Materials Testing and Research, Ueberlandstrasse 129, 8600 Duebendorf, Switzerland, General Energy Research Department, Paul Scherrer Institut, 5232 Villigen PSI, Switzerland

Received: February 13, 2009; Revised Manuscript Received: April 16, 2009

Laser-induced forward transfer is a powerful technique for the patterned deposition of thin layers. Sensitive materials can be transferred using an intermediate sacrificial layer, which protects the material from direct laser irradiation. Among various materials, triazene polymers are very promising sacrificial layers, and therefore, their ablation behavior has a particular importance for the transfer. The ablation behavior of a single sacrificial layer of a specific triazene polymer was investigated using time-resolved shadowgraphy to understand and optimize the deposition process. We analyzed the evolution of the shock wave generated by the decomposition of the triazene polymer to estimate the thermodynamics of the process. The energy balance shows that a large part of the energy is released into the shock wave but that thermal and mechanical losses predominate. On the other hand, the kinetic energy of the flyer corresponds only to a few percent of the total energy. We also observed a difference in the shock wave energy between front side and back side ablation when a flyer of undecomposed triazene polymer is ejected. The presence of the flyer diminishes the shock wave energy by a factor of 2 in the most extreme case.

Introduction

Laser-induced forward transfer (LIFT) is a deposition technique that allows the transfer of precise patterns of materials from a donor to a receiver substrate. The principle is based on the laser ablation of a thin film coated onto a transparent substrate (the donor). The donor film is ablated by a laser pulse impinging through the substrate and collected on a receiver plate facing the donor substrate. Precise transferred patterns, which are defined by the shape of the laser beam, are obtained in this way.[1−3]

In conventional LIFT, the material to transfer is directly irradiated by the laser pulse, which may be acceptable for metals.[4−6] However, there is a large interest in depositing sensitive materials, such as light-emitting polymers, which are degraded upon direct irradiation. This is possible by the introduction of a sacrificial layer between the donor film and the substrate. The role of the sacrificial layer is to absorb the laser pulse and, upon decomposition, to propel the intact donor layer. Inorganic absorbing materials (metals, ceramics) were already applied for this purpose, but the gas release is achieved only when the material is vaporized, which causes a pronounced heating of the transfer layer. Moreover, the high thermal conductivity of the absorbing material causes an even higher heat load on the top layer.

However, the purpose of the sacrifical layer is to propel the top layer with minimal heating. This is best achieved when a large amount of gas is released by photochemical decomposition and not by vaporization. A particulary suitable material for the sacrificial layer is a triazene polymer, which readily decomposes into gaseous fragments upon UV irradiation, therefore providing a large propulsion at a low laser fluence.[7−10] LIFT using a triazene sacrificial layer was first studied for the transfer of poly[methyl methacrylate].[8] Since, it has been successfully applied to transfer sensitive materials such as organic light-emitting diode pixels,[11] living cells[12] and nanocrystal quantum dots,[13] but is also suitable to deposit thin metallic films.[14]

In the previous examples, transfer was realized mainly when the donor and receiver substrates were in contact. This configuration is inappropriate for large area substrates or a successive multilayer deposition. Hence, efforts are now directed towards the deposition without contact. For this reason, it is important to understand how the material is ablated and transferred when the substrates are separated by a gap. A suitable method for this study is lateral time-resolved shadowgraphy imaging,[15] which is commonly used for imaging laser ablation processes[16−19] and, particularly, the material ejection in LIFT.[20−22]

In a preceding article, we presented shadowgraphy imaging of the front side and back side ablation of a single layer of the triazene polymer and showed that a polymer flyer was formed under certain conditions and that a shock wave was generated in all cases.[23] Shock waves are often used to initiate chemical reactions[24,25] and, in particular, decomposition reactions[26−29] to analyze the reaction kinetics. In this work, we proceed in the reverse way: we analyze the evolution of the shock wave generated from the decomposition of a triazene polymer to understand the thermodynamics of the reaction and of the complete process of laser-induced forward transfer. We calculated an energy balance to estimate the relative importance of the energy sources and consumption pathways, including the energies of the shock wave and the flyer.

Experimental

The chemical structure of the triazene polymer is shown in Chart 1 (top) and was synthesized according to a previously published procedure[30] (compound TP-6a). The polymer films were prepared on fused silica by spin-coating from chloroben-

† Part of the "Hiroshi Masuhara Festschrift".
* Corresponding author. E-mail: thomas.lippert@psi.ch.
‡ Empa.
§ Paul Scherrer Institut.

10.1021/jp901340s CCC: $40.75
Published on Web 05/18/2009

CHART 1: Chemical Structure of the Triazene Polymer (top) and of the Decomposition Fragments As Determined by Mass Spectrometry

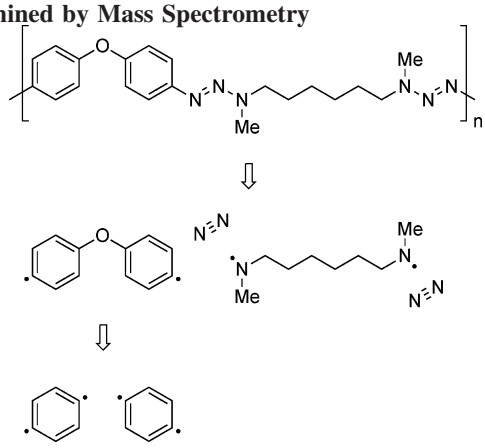

zene and cyclohexanone (1:1 w/w) solutions. The films were 460−500 nm thick, which is about 5 times the penetration depth of the laser.

The ablation experiments were performed with a pump−probe shadowgraphy setup to image the process at a nanosecond time-scale resolution. The pump laser was a XeCl excimer (Compex, Lambda Physik, $\lambda = 308$ nm, $\tau = 30$ ns), and single pulses were used. The ablation spot was defined by imaging a square mask onto the polymer film with a demagnification of 4, yielding a spot size of 500 μm. The sample was placed on a motorized translation stage with the film facing the laser beam for front side ablation and the opposite way for back side ablation. The fluence was controlled by an attenuator plate and measured by a pyroelectric energy meter (Molectron J4-09 or Gentec QE 50) placed at the end of the beamline. The film thickness and ablation depth were measured by profilometry (Ambios XP1), and the spot size, by optical microscopy.

Visualization of the process was achieved by a CMOS camera with a long-distance microscope objective placed perpendicular to the laser beam (i.e. parallel to the sample surface) with the focus at the ablation spot. Illumination was provided by the probe laser (Nd:YAG 2 ω, $\lambda = 532$ nm, $\tau = 5$ ns) pumping a fluorescent dye in a cuvette, which was placed on the camera axis on the opposite side of the sample. The delay between the pump and probe laser pulses was set by a digital pulse/delay generator (Stanford Research Systems DG535). A computer-controlled system allowed variation of the fluence, position, and time delay and took a sequence of pictures. Each picture was recorded with a different pulse and corresponds to a new position on the sample. From the calibrated pictures, the position of the features (shock wave and flyer) were measured perpendicularly to the sample surface.

Model

The calculation of an energy balance between the input and the output terms of the LIFT system allows analysis of the possible energy consumption pathways and evaluation of their relative importance. The input contributions are the incident laser energy (E_{laser}) and the decompostion energy of the ablated volume of triazene (E_{dec}). The output terms include the energy released into the shock wave (E_{SW}) and the kinetic energy of the flyer (E_{flyer}), which can be both evaluated from the shadowgraphy experiments. They also include terms much more difficult to quantify, such as the thermal and mechanical (shock propagation through the substrate) losses, as well as mechanical work to detach the flyer. All these unknown contributions are grouped into the energy losses, E_{loss}.

The energy balance is then

$$E_{laser} + E_{dec} = E_{SW} + E_{flyer} + E_{loss} \quad (1)$$

To compare the energies under different conditions, it is more practical to normalize eq 1 on its left-hand side,

$$1 = \eta_{SW} + \eta_{flyer} + \eta_{loss} \quad (2)$$

where η_i is the normalized energy of term i (i = SW, flyer, or loss), defined by

$$\eta_i = \frac{E_i}{E_{laser} + E_{dec}} \quad (3)$$

The incident energy is given by

$$E_{laser} = A \cdot \Phi_{laser} \cdot T \quad (4)$$

where A is the ablated area and Φ_{laser} is the laser fluence. T is the transmittance corrected for the reflection at the air/polymer interface during front side irradiation and at the air/substrate and substrate/polymer interfaces during back side irradiation. Although the polymer surface changes dynamically during the laser pulse, this aspect was not considered for the sake of simplicity. The decomposition energy is calculated from the decomposition enthalpy of the polymer $\Delta_{dec}H$. The value is strictly valid only for an isobaric transformation, but this approximation was also used by other authors.[26,31] The decomposition energy is

$$E_{dec} = \Delta_{dec}H \cdot m = \Delta_{dec}H \cdot \rho_f A d \quad (5)$$

with m being the mass of the ablated polymer film; ρ_f, its density; and d, the ablated depth. The density has been measured in a previous work.[32] The ablation depth was measured by profilometry after front side ablation.

The energy of the shock wave was evaluated by the planar model developed by Freiwald.[33] It was applied for analyzing the ablation of a similar triazene polymer[31] and found to be more appropriate than a model accounting for the hemispherical geometry.[34] The model includes the energy of the released gaseous debris, E_{debris}, and the energy transferred to the surrounding gas, E_{gas}. The energy of the shock wave is given by

$$E_{SW} = E_{debris} + E_{gas} \quad (6)$$

$$= \left[\frac{Ad}{8}\left(\frac{2}{\gamma+1}\right)^2 \rho_f\right] v^2 + \left[\frac{\rho_g A}{\gamma+1}\left(\frac{1}{\gamma-1} + \frac{4}{\gamma+1}\right)\right] v^2 x \quad (7)$$

where ρ_g is the density of the surrounding atmosphere and γ is its adiabatic ratio. In this work, we added a parameter, t_0, to allow for a delayed observation of the origin of the shock wave.[35,36] The position as a function of time is given by

$$x = \frac{\left(\frac{2}{3}C_5 E_{SW}^{\frac{1}{2}}(t - t_0) + C_4^{\frac{3}{2}}\right)^{\frac{2}{3}} - C_4}{C_5} \quad (8)$$

with

$$C_4 = \frac{Ad}{8}\left(\frac{2}{\gamma + 1}\right)^2 \rho_f \quad (9)$$

$$C_5 = \frac{\rho_g A}{\gamma + 1}\left(\frac{1}{\gamma - 1} + \frac{4}{\gamma + 1}\right) \quad (10)$$

C_4 and C_5 are known, and the fit of x versus t yields E_{SW} and t_0.

The kinetic energy of the flyer, E_{flyer}, is calculated from the initial velocity and the mass using

$$E_{flyer} = \frac{1}{2}\rho_f A h \cdot v_{flyer}^2 \quad (11)$$

where the flyer thickness, h, was calculated from the film thickness minus the ablated depth, d. One assumption used in this calculation is that the ablated thickness of triazene upon back side irradiation corresponds to the ablation depth measured for front side ablation at the corresponding fluence. This assumption may be not quite accurate because of different heat diffusion geometries, but it is simple and gives a value that can be measured directly.

Results and Discussions

The laser ablation of the triazene polymer was studied with the laser impinging from the front side and from the back side (through the transparent substrate), the latter being the configuration used for LIFT. The purpose of this approach was to compare the shock wave evolution in both cases and to evaluate the energy released from the process. The propagation velocity of the shock wave and flyer were measured, and the model shown above then allows an estimation of the energy of these objects and a comparison with the input energy.

Shock Wave Propagation. The position of the shock wave was measured from the images and plotted versus the time elapsed after the beginning of the ablation pulse (Figure 1). The lines are fit curves, as explained below. The data for front and back side irradiation are shown for high (700 mJ/cm^2) and low fluence (50 mJ/cm^2). The latter fluence was chosen because it is just above the ablation threshold for a complete film delamination upon back side irradiation.[23]

The shock waves exhibit a typical deceleration due to the distribution of the initial energy into an increasing volume of air. The velocity of the shock wave is, as expected, faster at the higher fluence. However, two features are remarkable. The trajectories for front side and back side ablation overlap well at the high fluence but are clearly different at 50 mJ/cm^2. The second interesting observation is that the shock waves do not seem to start at the same time, if we consider the apparent interception of the trajectories with the time axis ($x = 0$) as the starting time of the shock wave propagation. At 50 mJ/cm^2, the shock generated by back side ablation seems to start hundreds of nanoseconds after the shock wave generated by front side irradiation. We can exclude an artifact of the measurement, because the uncertainty on the time is much less than the observed shift. Moreover, a systematic error between front and back side measurements would not explain the difference between the curves, because a shift of all curves for back side with respect to front side curves would shift the difference to other fluences but not cancel it.

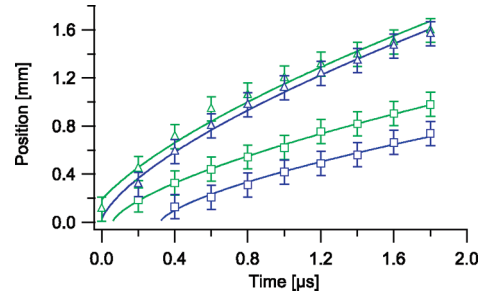

Figure 1. Points: position of the shock wave front versus time measured perpendicular to the sample for front side (green) and back side ablation (blue), each at two fluences: (Δ) 700 and (□) 50 mJ/cm^2. Lines: corresponding fit curves from eq 8.

The main difference between front side and back side ablation at low fluences is the presence of a flyer in the latter case.[23] This layer of undecomposed polymer is ejected when the fluence is not high enough to ablate the whole triazene film, yet is sufficient to delaminate and propel the remaining part. Thicker flyers are obtained at fluences just above the delamination threshold; that is, the minimum fluence required for complete material removal from the ablated spot.[14] For a given layer thickness of 460 nm, the threshold fluence is between 40 and 50 mJ/cm^2.[23] Interestingly, the fluence range at which the major differences in the shock wave evolution appear is where a thick material flyer is ejected. When the fluence is increased, the flyer becomes thinner until it is not visible anymore (at 700 mJ/cm^2) and, correspondingly, the trajectories of the shock wave tend to overlap. It is clear that the shock wave evolution is directly related to the flyer thickness. The energies involved in the processes are now analyzed to understand the phenomenon.

Energy Balance. The energy balance is obtained by evaluation of the input and the output terms. The input energy is discussed first, with an emphasis on the triazene polymer.

Input Energy. In addition to be a protective layer against thermal and photochemical load for the transfer material, the main purpose of the sacrificial layer is to convert the laser energy (radiation) into a useful mechanical energy (thrust). The suitability and selection of the material for laser ablation is therefore extremely important. The triazene polymer, which was specifically designed for laser ablation at 308 nm,[9] is a very good candidate for these requirements. This wavelength is suited best for a commercial application of excimer lasers, mainly due to the lifetime of the gases and optical components.

The triazene polymer incorporates a photosensitive group in the main chain, which ensures a clean decomposition into small, gaseous molecules. The triazene polymer reveals the most promising properties for laser ablation, that is, a very high ablation rate as compared to other polymers used in laser ablation.[37] It exhibits a clean ablation behavior without any redeposition of decomposition fragments and carbonization of the crater, different from other polymers (e.g., polyimide) that can be ablated at an irradiation wavelength of 308 nm.[38]

This behavior is due to a pronounced photochemical component in the ablation mechanism of the triazene polymer. Although a strict separation between a photothermal or a photochemical character is not relevant, some measurements have shown evidence of an important phototchemical part; for

TABLE 1: Fit Parameters

name	symbol	value	unit
area	A	$2.5 \cdot 10^{-7}$	m^2
front side transmittance	T	0.905	
back side transmittance	T	0.902	
decomposition enthalpy	$\Delta_{dec}H$	$6.97 \cdot 10^5$	J/kg
adiabatic ratio	γ	1.4	
density of triazene	ρ_f	$1.12 \cdot 10^3$	kg/m^3
density of air	ρ_g	1.184	kg/m^3

instance, the presence of metastable N_2 in the decomposition product[39] or the fact that material removal happens only during the laser pulse[16,40] and not delayed, as is the case for a photothermal decomposition.[41]

The decomposition reaction, shown in Chart 1, is exothermic and starts with a homolytic bond breaking of the triazene unit, followed by a subsequent fragmentation, as revealed by mass spectrometry.[42] The decomposition releases a large amount of gaseous products, and at least four to six gaseous fragments (including two N_2 molecules) are formed per repetition unit. Therefore, a huge pressure jump is created at the ablation spot during the time scale of the laser pulse, which can be converted into mechanical energy (pressure work). The number of fragments allows an estimation of the initial pressure created at the ablation spot prior to expansion using the ideal gas law. A pressure jump on the order of 0.5−1 GPa can be estimated for the conditions of this work. This value is based on the assumption of four fragments, which is the lowest limit; therefore, the actual pressure may be even much higher.

The energy of the process originates from two sources: the laser energy and the exothermic decomposition of the triazene polymer, which has been determined previously.[43] The calculations show that the laser energy is much more important than the decomposition energy, which is always <15% of the total energy. This reveals that the important feature of the triazene polymer for LIFT is not the exothermic decomposition but the production of a large amount of gas, therefore creating a strong pressure jump.

Output Energy. We start with the analysis of the shock wave, which is the main energy output and which is always present. The energy released in a shock wave can be computed from its trajectory. The positions are fitted versus time with eq 8, and the results are shown as solid lines in Figure 1. The applied parameters are summarized in Table 1. We noticed that the value for the ablated thickness had only a very minor influence on the calculated energy of the shock wave. This is due to the predominance of the C_5 term in the shock wave equation and the low contribution of the exothermal decomposition energy of the polymer to the total energy.

The best fit is obtained at intermediate fluences (not shown), whereas at the highest fluence, the fit line is less curved than the actual data points, suggesting that a hemisherical model would be slightly more suitable in this case.[31] The data points at 50 mJ/cm^2 are correspondingly more linear than the fit line, probably because the shock wave weakens when the fluence gets closer to the ablation threshold. Eventually, it converges to a plain sound wave that propagates linearly.[44] However, the same model was applied for all fluences to obtain consistent data.

The fit provides two parameters: the time delay, t_0, discussed below; and the initial energy, E_{SW}. This energy is plotted versus the incident laser fluence in Figure 2 for both front side and back side ablation. The shock wave energy increases as expected with the fluence with both curves following the same trend.

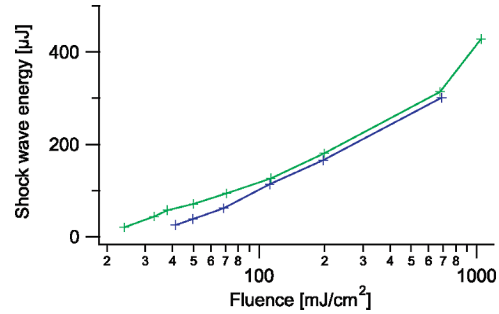

Figure 2. Shock wave energy versus laser fluence for front side (green) and back side ablation (blue). The lines are guides for the eyes.

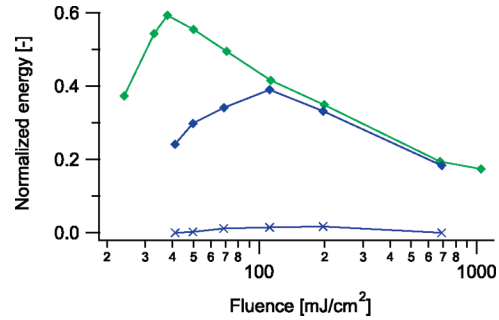

Figure 3. Normalized energy versus laser fluence for the shock wave at front side (green) and back side ablation (blue), as well as for the flyer in the case of back side ablation (×). The lines are guides for the eyes.

However, the shock wave energy for front side irradiation is consistently higher and pronounced differences are observed at low fluences. A representation of the normalized energies, according to eq 3, is better suited to enhance this difference.

Figure 3 (◇) shows the normalized shock wave energies versus incident fluence. A value of 1 corresponds to a complete transfer of the input energy into the shock wave. The data point at the lowest fluence corresponds to no ablation (front) or no flyer ejection (back) for each curve.

The energy of the shock wave lies between 20% and 60% of the total energy. This order of magnitude is realistic, and the values reveal that a significant part of the energy goes into the loss processes described above. However, the fact that up to 60% of the input energy (laser plus chemical energy) is converted into mechanical energy shows that the ablation of the triazene polymer is an efficient source of mechanical energy. Both curves reveal a maximum value, although at a higher fluence for back side irradiation. It is not yet clear why a maximum is reached, but this may be related to the procedure of calculating the laser energy. For this calculation, we assume that the laser light is completely absorbed, which may be incorrect at low and high fluences, for the reasons discussed below.

At low fluences, the laser pulse is inefficient to create a shock wave. Indeed, when the fluence decreases and gets close to the threshold fluence, a dramatic decrease in the ablation depth occurs, being eventually zero at the threshold. The volume of released gas decreases accordingly. The shock wave is created by a pressure jump at the ablation spot, which is provided by the volume increase and the thermal expansion of the materials. When the gas volume diminishes, the shock wave is weaker.

At high fluences, only a part of the laser pulse energy is absorbed. At these fluences, the ablation depth is similar to the film thickness, and a part of the laser light is transmitted through the sample, thus decreasing the energy available in the balance.

This fact can be taken into account, but it was noticed that applying the linear absorption coefficient for the energy calculation results in unrealistic values (>100%) at low fluences, where the affected thickness tends to zero. Indeed, a shock wave was even visible at 24 mJ/cm^2 where no ablation was detected. For this reason, we believe that the incident pulse energy is a good yet simple value for the calculation.

More interesting is the comparison between both curves. The trend seen in Figure 2 appears even more clearly in Figure 3; that is, a difference of a factor of 2 for the shock wave energy at low fluences between front side and back side irradiation. The largest difference is observed at 40 mJ/cm^2, where for back side irradiation, a part of the film is decomposed but no flyer is ejected. When the fluence is increased, the difference decreases until vanishing at 110 mJ/cm^2, corresponding to a estimated flyer thickness of 50% of the original film.

One possible approach to explain these data is to take the kinetic energy of the flyer into account. The flyer position was therefore measured and fitted versus time with a linear relation (not shown). The slope of this line gives the velocity, v_{flyer}, used in eq 11 to calculate the kinetic energy of the flyer. The obtained normalized energy is included in Figure 3. The calculated maximum value was below 2%, which is much too low to explain the difference in the shock wave energies. Moreover, the maximum of the curve is found at 200 mJ/cm^2, where both shock waves have the same energy. The energy used to accelerate the flyer does therefore not explain the observed difference.

Another possible explanation may originate from the different geometries of both systems. They are very different at low fluences, which has implications for the heat transfer and the mechanical energy. We have previously shown that highly thermally conductive substrates, such as fused silica, are major heat sinks during ablation of films thinner than 50 nm.[32] When ablation is performed from the front, energy losses occur by the heat transfer through the remaining polymer layer and further into the fused silica. However, the influence of the substrate is low because the triazene thermally insulates the ablated area. The case is different during back side ablation. The decomposed zone is located between the remaining triazene layer and the fused silica, which acts as a heat sink. It can be expected that an important part of the thermal energy is lost into the fused silica because the ablated zone is not insulated from the substrate. At high fluences, the undecomposed triazene layer is thinner or zero, and the two irradiation geometries are similar. This effect can explain the observed difference quite well.

The mechanical processes are different between front side and back side ablation, as well. During front side ablation, the ablation products are freely ejected into the atmosphere, and mechanical losses happen only by the shock wave recoil into the substrate. But when a flyer is ejected upon back side ablation, the edges of the flyer have to be detached from the surrounding film, which requires additional energy. Further investigations are being carried out to quantify this amount, which may be even used to obtain the "strength" of a material. Moreover, the shock wave is created in the ablated zone (i.e. between the flyer and the substrate) but is observed in front of the flyer. The shock wave must therefore travel through the polymer film, which will be the flyer, before propagating into the ambient air and may loose energy by heating the polymer during this crossing. This possibility is discussed further to explain differences of the observation time in the shock wave appearance.

Finally, another reason for the weaker shock wave in the presence of a flyer may be a partial reflection of the shock wave at the polymer/air interface when the shock wave reaches the external film surface after traveling through the undecomposed layer, which may cause an additional energy loss.

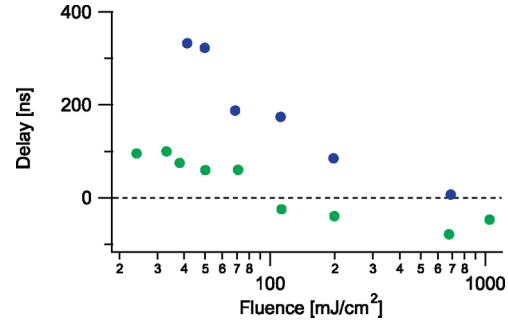

Figure 4. Delay of the apparent time origin of the shock wave with respect to the ablation pulse (parameter t_0 from fit), plotted versus laser fluence for front side (green) and back side ablation (blue). A positive delay represents an origin after the laser pulse.

Delay. As seen in Figure 1, the shock waves are best approximated when a time delay is introduced into the fit equation. These t_0 values are shown in Figure 4 for front side and back side ablation. A positive delay means that the shock wave is observed after the laser pulse (reference point at the top of the main intensity peak).

An increasing delay time is observed for decreasing fluences, and the delay is larger for back side irradiation. The delay is negative at high fluence for front side ablation, which is, of course, unreasonable. It indicates that the model does not describe the early data points correctly. At the low fluences, however, the trend is in accordance with the observed shock wave trajectories; that is, shock waves generated by front side irradiation start earlier than those from back side ablation.

The reason for this difference in the delay is not clear. Even the sound propagation in the flyer, which may be slower than in air, cannot explain it. Assuming a speed of sound for a rubberlike material (~40 m/s), which is the extreme case for a slow propagation medium, the time for crossing an entire flyer would be only around 10 ns, which is at least 1 order of magnitude shorter than the observed time delay. There may be other reasons responsible for this delay that are related to the geometry of the cavity where the flyer is formed.

The explanation may also be related to the domain of validity of the equation describing the shock wave. The delay may correspond to the time the shock front needs to reach a hemispherical shape, where the equation can describe the data points very well. Before this time, the geometry of the shock wave is still transient and the fit equation may not able to describe the points correclty. This possibility has been suggested by other authors, as well.[35,36]

Conclusions

The calculation of an energy balance on the front side and back side ablation of a triazene polymer layer was realized by a thermodynamical analysis of the input energy as well as an evaluation of the consumption pathways. The order of magnitude obtained suggests a reliable analysis. The main source of energy is the laser and not the exothermic decomposition of the polymer. A large part of the energy is dissipated into the shock wave, showing an efficient conversion of the laser energy into mechanical energy (20−60%). The remaining energy consumption occurs by other processes, such as thermal and mechanical losses. The propulsion of the flyer, which is the useful energy

for LIFT, represents only a few percent of the total energy delivered to the system.

It was found that the shock wave energy is dependent on the configuration; that is, the shock wave generated upon back side ablation can be 2 times as weak as for the front side irradiation. The most pronounced difference between the two cases is obtained when a thick flyer of undecomposed polymer is ejected, thereby revealing the influence of the flyer on the shock wave propagation. The present study was realized on a single sacrificial layer of triazene polymer and can now serve as a reference for comparison with more complex cases. Systems made of a stack of a sacrifical layer and transfer material layer are currently under investigation. This next step will improve our understanding of the energy dissipation mechanisms in LIFT, which is an important point to achive gentle material deposition. The analysis tools can be refined also, and some more complex calculations with 2D hydrodynamic models will help in the better understanding of the system.

Acknowledgment. Financial support from the Swiss National Science Foundation is gratefully acknowledged.

References and Notes

(1) Bohandy, J.; Kim, B. F.; Adrian, F. J. *J. Appl. Phys.* **1986**, *60*, 1538–1539.
(2) Kyrkis, K.; Andreadaki, A.; Papazoglou, D.; Zergioti, I. Direct transfer and microprinting of functional materials by laser-induced forward transfer. In *Recent Advances in Laser Processing of Materials*; Perrière, J.; Millon, E.; Fogarassy, E., Eds.; Elsevier: Amsterdam, New York, 2006; pp 213−241.
(3) Arnold, C.; Serra, P.; Piqué, A. *MRS Bull.* **2007**, *32*, 23–31.
(4) Zergioti, I.; Mailis, S.; Vainos, N.; Fotakis, C.; Chen, S.; Grigoropoulos, C. *Appl. Surf. Sci.* **1998**, *127−129*, 601–605.
(5) Sano, T.; Yamada, H.; Nakayama, T.; Miyamoto, I. *Appl. Surf. Sci.* **2002**, *186*, 221–226.
(6) Banks, D. P.; Grivas, C.; Mills, J. D.; Eason, R. W.; Zergioti, I. *Appl. Phys. Lett.* **2006**, *89*, 193107–3.
(7) Karnakis, D.; Lippert, T.; Ichinose, N.; Kawanishi, S.; Fukumura, H. *Appl. Surf. Sci.* **1998**, *127−129*, 781–786.
(8) Mito, T.; Tsujita, T.; Masuhara, H.; Hayashi, N.; Suzuki, K. *Jpn. J. Appl. Phys., Part 2* **2001**, *40*, L805–L806.
(9) Lippert, T.; Dickinson, J. *Chem. Rev.* **2003**, *103*, 453–485.
(10) Lippert, T. *Adv. Polym. Sci.* **2004**, *168*, 51–246.
(11) Fardel, R.; Nagel, M.; Nüesch, F.; Lippert, T.; Wokaun, A. *Appl. Phys. Lett.* **2007**, *91*, 061103.
(12) Doraiswamy, A.; Narayan, R.; Lippert, T.; Urech, L.; Wokaun, A.; Nagel, M.; Hopp, B.; Dinescu, M.; Modi, R.; Auyeung, R.; Chrisey, D. *Appl. Surf. Sci.* **2006**, *252*, 4743–4747.
(13) Xu, J.; Liu, J.; Cui, D.; Gerhold, M.; Wang, A. Y.; Nagel, M.; Lippert, T. K. *Nanotechnology* **2007**, *18*, 025403.
(14) Fardel, R.; Nagel, M.; Nüesch, F.; Lippert, T.; Wokaun, A. *Appl. Surf. Sci.* **2007**, *254*, 1322–1326.
(15) Settles, G. *Schlieren and shadowgraphy techniques: visualizing phenomena in transparent media*; Springer-Verlag: Berlin, 2001.
(16) Hauer, M.; Funk, D. J.; Lippert, T.; Wokaun, A. *Appl. Phys. A: Mater. Sci. Process.* **2003**, *77*, 297–301.
(17) Dlott, D. D. *Appl. Surf. Sci.* **2002**, *197−198*, 3–10.
(18) Furutani, H.; Fukumura, H.; Masuhara, H.; Kambara, S.; Kitaguchi, T.; Tsukada, H.; Ozawa, T. *J. Phys. Chem. B* **1998**, *102*, 3395–3401.
(19) Fukumura, H.; Takahashi, E.; Masuhara, H. *J. Phys. Chem.* **1995**, *99*, 750–757.
(20) Hopp, B.; Smausz, T.; Barna, N.; Vass, C.; Antal, Z.; Kredics, L.; Chrisey, D. *J. Phys. D: Appl. Phys.* **2005**, *38*, 833–837.
(21) Young, D.; Auyeung, R. C. Y.; Piqué, A.; Chrisey, D. B.; Dlott, D. D. *Appl. Surf. Sci.* **2002**, *197−198*, 181–187.
(22) Zergioti, I.; Karaiskou, A.; Papazoglou, D.; Fotakis, C.; Kapsetaki, M.; Kafetzopoulos, D. *Appl. Surf. Sci.* **2005**, *247*, 584–589.
(23) Fardel, R.; Nagel, M.; Nüesch, F.; Lippert, T.; Wokaun, A. *Appl. Surf. Sci.* **2009**, *255*, 5430–5434.
(24) Tsuboi, Y. *J. Phys. Chem. A* **2008**, *112*, 6517–6521.
(25) Croce, A. E. *Phys. Chem. Chem. Phys.* **1999**, *1*, 5345–5351.
(26) Ben-Eliahu, Y.; Haas, Y.; Welner, S. *J. Phys. Chem.* **1995**, *99*, 6010–6018.
(27) Hippler, H. *J. Chem. Phys.* **1995**, *103*, 3510–3516.
(28) Gruzdkov, Y. A. *J. Phys. Chem. A* **2008**, *112*, 3947–3952.
(29) Patterson, J. E. *J. Phys. Chem. A* **2008**, *112*, 7374–7382.
(30) Nagel, M.; Hany, R.; Lippert, T.; Molberg, M.; Nüesch, F.; Rentsch, D. *Macromol. Chem. Phys.* **2007**, *208*, 277–286.
(31) Bennett, L.; Lippert, T.; Furutani, H.; Fukumura, H.; Masuhara, H. *Appl. Phys. A: Mater. Sci. Process.* **1996**, *63*, 327–332.
(32) Fardel, R.; Nagel, M.; Nüesch, F.; Lippert, T.; Wokaun, A.; Luk'yanchuk, B. *Appl. Phys. A: Mater. Sci. Process.* **2008**, *90*, 661–667.
(33) Freiwald, D. A. *J. Appl. Phys.* **1972**, *43*, 2224–2226.
(34) Freiwald, D. A.; Axford, R. A. *J. Appl. Phys.* **1975**, *46*, 1171–1174.
(35) Ohkoshi, M.; Yoshitake, T.; Tsushima, K. *Appl. Phys. Lett.* **1994**, *64*, 3340–3342.
(36) Gonzalo, J.; Afonso, C. N.; Madariaga, I. *J. Appl. Phys.* **1997**, *81*, 951–955.
(37) Wei, J.; Hoogen, N.; Lippert, T.; Nuyken, O.; Wokaun, A. *J. Phys. Chem. B* **2001**, *105*, 1267–1275.
(38) Raimondi, F.; Abolhassani, S.; Brutsch, R.; Geiger, F.; Lippert, T.; Wambach, J.; Wei, J.; Wokaun, A. *J. Appl. Phys.* **2000**, *88*, 3659–3666.
(39) Hauer, M.; Dickinson, T.; Langford, S.; Lippert, T.; Wokaun, A. *Appl. Surf. Sci.* **2002**, *197*, 791–795.
(40) Furutani, H.; Fukumura, H.; Masuhara, H.; Lippert, T.; Yabe, A. *J. Phys. Chem. A* **1997**, *101*, 5742–5747.
(41) Masubuchi, T.; Tada, T.; Nomura, E.; Hatanaka, K.; Fukumura, H.; Masuhara, H. *J. Phys. Chem. A* **2002**, *106*, 2180–2186.
(42) Lippert, T.; Langford, S.; Wokaun, A.; Georgiou, S.; Dickinson, J. *J. Appl. Phys.* **1999**, *86*, 7116–7122.
(43) Lippert, T.; Bennett, L.; Nakamura, T.; Niino, H.; Ouchi, A.; Yabe, A. *Appl. Phys. A: Mater. Sci. Process.* **1996**, *63*, 257–265.
(44) Zel'dovich, Y. B.; Raizer, Y. P. *Physics of shock waves and high-temperature hydrodynamic phenomena*; Dover Publications: Mineola, N.Y., 2002.

JP901340S